

RESEARCH

Open Access



Posttranscriptional RNA stabilization of telomeric RNAs FRG2, DBE-T, D4Z4 at human 4q35 in response to genotoxic stress and D4Z4 macrosatellite repeat length

Valentina Salsi¹, Francesca Losi¹, Monica Salani², Paul D. Kaufman³ and Rossella Tupler^{1*}

Abstract

Background Reduced copy number of the D4Z4 macrosatellite at human chromosome 4q35 is associated with facioscapulohumeral muscular dystrophy (FSHD). A pervasive idea is that chromatin alterations at the 4q35 locus following D4Z4 repeat unit deletion lead to disease via inappropriate expression of nearby genes. Here, we sought to analyze transcription and chromatin characteristics at specific regions of 4q35 and how these are affected by D4Z4 deletions and exogenous stresses.

Results We found that the 4q subtelomere is subdivided into discrete domains, each with characteristic chromatin features associated with distinct gene expression profiles. Centromeric genes within 4q35 (*SLC25A4*, *FAT1* and *FRG1*) display active histone marks at their promoters. In contrast, poised or repressed markings are present at telomeric loci including *FRG2*, *DBE-T* and *D4Z4*. We discovered that these discrete domains undergo region-specific chromatin changes upon treatment with chromatin enzyme inhibitors or genotoxic drugs. We demonstrated that the 4q35 telomeric *FRG2*, *DBE-T* and *D4Z4*-derived transcripts are induced upon DNA damage to levels inversely correlated with the D4Z4 repeat number, are stabilized through posttranscriptional mechanisms upon DNA damage and are bound to chromatin.

Conclusion Our study reveals unforeseen biochemical features of RNAs from clustered transcription units within the 4q35 subtelomere. Specifically, the *FRG2*, *DBE-T* and *D4Z4*-derived transcripts are chromatin-associated and are stabilized posttranscriptionally after induction by genotoxic stress. Remarkably, the extent of this response is modulated by the copy number of the D4Z4 repeats, raising new hypotheses about their regulation and function in human biology and disease.

Keywords D4Z4 chromatin signature, DNA damage, Epigenetic regulation, FSHD

*Correspondence:

Rossella Tupler

rossella.tupler@unimore.it

Full list of author information is available at the end of the article



© The Author(s) 2025. **Open Access** This article is licensed under a Creative Commons Attribution-NonCommercial-NoDerivatives 4.0 International License, which permits any non-commercial use, sharing, distribution and reproduction in any medium or format, as long as you give appropriate credit to the original author(s) and the source, provide a link to the Creative Commons licence, and indicate if you modified the licensed material. You do not have permission under this licence to share adapted material derived from this article or parts of it. The images or other third party material in this article are included in the article's Creative Commons licence, unless indicated otherwise in a credit line to the material. If material is not included in the article's Creative Commons licence and your intended use is not permitted by statutory regulation or exceeds the permitted use, you will need to obtain permission directly from the copyright holder. To view a copy of this licence, visit <http://creativecommons.org/licenses/by-nc-nd/4.0/>.

Introduction

Repetitive DNA sequences occur in multiple copies and comprise over 50% of the human genome [1, 2]. DNA repeats can be categorized based on their size and copy number: high-frequency repeats, also known as satellite DNA sequences, are found in various loci, including pericentromeric, subtelomeric and interstitial regions. Satellites typically form constitutive blocks of heterochromatin, notably at telomeres, centromeres and at the short arms of acrocentric chromosomes. Although most satellites (~89.5%) are located within repressive chromatin domains, multiple studies have found that these elements have significant impacts on evolution, genetic variation and gene expression regulation [3, 4].

FSHD had previously been correlated with reduction of macrosatellite D4Z4 repeats at the 4q35 subtelomere [5] and aberrant expression of nearby genes [6]. In 2010, a unifying model has been proposed to explain the molecular basis of FSHD [7], stating that deletion of 4q D4Z4 repeats must be combined with a polyadenylation polymorphism at the most telomeric D4Z4 copy to create a FSHD-predisposing signature. This configuration stabilizes transcripts encoding the DUX4 transcription factor, driving disease-related gene expression.

Studies investigating D4Z4 chromatin have detected multiple repressive modifications, including DNA methylation [8–14], di/trimethylation of histone H3 at lysine 9 (H3K9me2/3) [15–17], trimethylation of histone H3 at lysine 27 (H3K27me3) [18] and association of the related chromatin proteins CBX3/HP1 γ and EZH2 [18]. Proteomic analyses of proteins associated with the D4Z4 revealed that the NuRD and CAF-1 complexes are crucial for maintaining DUX4 repression [19].

Moreover, D4Z4 recruits a multi-protein repressor complex, the D4Z4 recognition complex (DRC), whose removal is associated with increased expression of 4q35 genes [6]. In the current patho-physiological model for FSHD [20], reduction of the D4Z4 array causes a loss of repressive histone modifications and the ectopic expression of *DUX4*, a retrogene present in each D4Z4 unit [21, 22]. Functional, full-length DUX4 transcripts are produced from the last D4Z4 unit when they are stabilized in individuals carrying a permissive 4qA haplotype that includes a polyadenylation signal (in the pLAM sequence) near the most telomere-proximal D4Z4 unit [21]. For this reason, the majority of studies of epigenetic mechanisms in FSHD focus on the D4Z4 last repeat [7].

Despite the seemingly straightforward nature of this model for FSHD, the progressive accumulation of clinical and epidemiological data over the years, along with the advent of new technologies and new genome assemblies, has highlighted the limitations of this model. In particular, the unifying model fails to adequately account for the

incomplete penetrance recorded in individuals who carry the 4q35 FSHD molecular signature [23–28]. It is now known that D4Z4-deleted alleles containing the polyadenylation polymorphism are present in approximately 2% of the human population and in 4.6% of human pangenomes haplotypes, akin to highly frequent polymorphism [29, 30]. The complexity of FSHD is also highlighted by genotype–phenotype correlation studies, in which several clinical phenotypes ranging from asymptomatic carriers to wheelchair-bound patients are observed [23–26, 28, 31–36]. Thus, the current model for FSHD pathogenesis does not capture the additional factors and mechanisms playing a role in FSHD onset and development. We thus reasoned that exploring the transcription of selected 4q35 genes, together with the epigenetic setting associated with it, might help fill gaps in our understanding of FSHD.

As in reality chromatin constitution and gene expression vary to adjust to “environmental changes” occurring constantly in a complex biological system, by quantifying RNA levels and analyzing chromatin characteristics at this locus, we aimed at gaining insights into the mechanisms of chromatin remodeling, and how this process influences gene expression in both healthy and diseased states in response to changes. Moreover, changes of chromatin conformation and gene expression in response to external stimuli, such as exogenous stresses, help to explore how environmental factors can influence genetic predisposition and cellular responses, an approach which is pivotal for understanding disease progression and adaptation mechanisms.

Here, we characterize dynamic regulatory events at different loci of selected 4q35 genes. Different patterns of histone modifications correlate with the differential transcriptional responses to genotoxic stress. In particular, we found that the most telomeric 4q35 transcripts are chromatin-associated and their levels are increased upon treatments with DNA damaging agents due to posttranscriptional stabilization. These latter properties are affected by the size of the subtelomeric D4Z4 array. Collectively, our results highlight that 4q35 constitutes a multipartite genomic locus providing distinct modes of regulation in response to external cues. These responses correlate with D4Z4 size, thus providing additional elements to define the biological role of subtelomeric repeats and how they can be associated with anomalous responses, leading to disease.

Results

Chromatin and transcription analysis of the 4q35 region reveals distinct epigenetic patterns

To investigate the mechanism(s) by which the D4Z4 macrosatellite array affects the transcriptional regulation

of the 4q35 locus (Fig. 1A), we measured RNA levels of genes associated with FSHD located at different distances from the D4Z4 array. On the centromeric side of 4q35, we analyzed RNAs from these protein-coding genes (Fig. 1A): *SLC25A4* (*Adenine Nucleotide Transporter 1*; known also as *Solute carrier family 25 member 4 SLC25A4*), *FAT1* (*FAT atypical cadherin 1*) and *FRG1* (*FSHD region gene 1*), which are positioned at 4.9 Mb, 3.5 Mb and 127 kb from the D4Z4 array, respectively. We also analyzed telomeric RNAs, including *FRG2* (*FSHD region gene 2*; 37 kb from the array), and *DBE-T* (*D4Z4 Binding Element-Transcript*), a lncRNA transcribed from the 5' end of the D4Z4 array. We also analyzed two additional transcripts derived from D4Z4: DUX4 exon1 (Ex1)-containing transcripts, hereafter named D4Z4-T (D4Z4-Transcript), which arise from each D4Z4 repeat, and DUX4-FL (DUX4 Full Length) pLAM-containing

transcripts, the FSHD disease-associated mRNAs derived from the most telomeric D4Z4 repeat (Fig. 1A and Supplemental_Fig_S1). We analyzed human primary myoblasts (HPMs) and trophoblast-derived cells (HTCs) obtained from FSHD subjects heterozygous for a D4Z4 reduced allele (DRA) and matched controls (Supplemental_Table_M3) [37]. We chose human trophoblast-derived cells (HTCs) for this study because they serve as a relevant model for early developmental gene expression, as they are not yet committed to a specific lineage, which is crucial since several genes in the 4q35 locus, including DUX4, may be active during early embryonic development.

We evaluated our primer sets both by performing in silico PCR using the T2T-CHM13 genome assembly and through the amplification of genomic DNA and cDNA derived from human/rodent monochromosomal hybrid

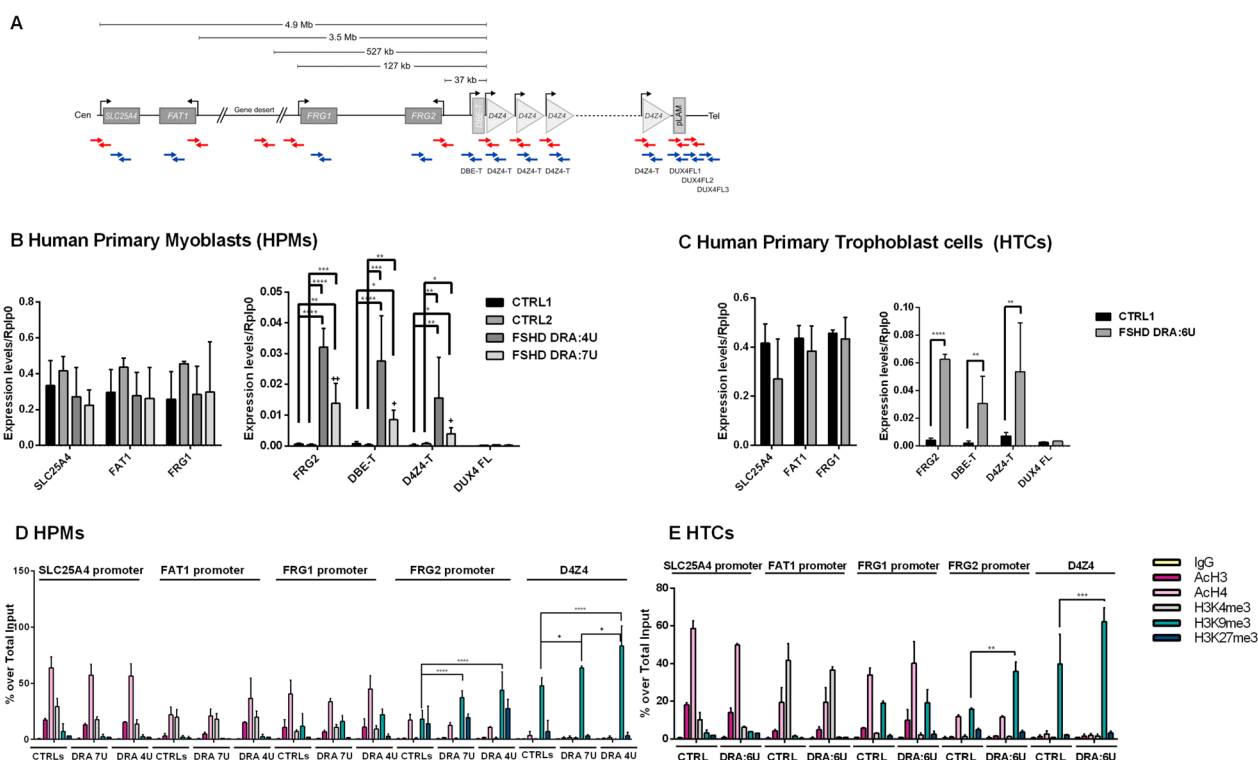


Fig. 1 4q35 genes expression and epigenetic profile. **A** Schematic representation of chromosome 4q35 showing physical distances between *SLC25A4*, *FAT1*, *FRG1* and *FRG2* genes and the D4Z4 macrosatellite within the AF146191-U85056 contig, based on GenBank entry U85056.1. The positions of primers used in ChIP experiments (red) and qPCR (blue) are shown. **B–C** RT-qPCR quantification of *SLC25A4*, *FAT1*, *FRG1*, *FRG2*, *DBE-T*, *D4Z4-T* and *DUX4-FL* mRNAs in **(B)** human primary myoblasts (HPMs) and **(C)** human trophoblast cells (HTCs). Data were normalized using RPLP0 as a reference mRNA. **D, E** Chromatin immunoprecipitation (ChIP) analysis performed in **D** HPMs and **E** HTCs. IPs were performed using the indicated antibodies recognizing H3K4me3, H3K9me3, H3K27me3 and pan-acetylated Histone 3 and 4 (AcH3 and AcH4), or a non-specific control (IgG), followed by qPCR amplification using primers described in Fig. 1A. Data are displayed as the percent enrichment for each antibody over total input chromatin. The values of the CTRL samples CTRLs ($n=3$) and FSHD DRA:4U ($n=2$) were averaged. Experiments were done in triplicate and analyzed using two-way ANOVA statistical tests. Asterisks show the statistical significance of DRA cells compared to control cells, while plus signs show the significance of DRA 4U compared to DRA 7U for each antibody, as follows: *, $+0.05 < p\text{-value} < 0.01$; **, $+0.01 < p\text{-value} < 0.001$; ***, $+0.001 < p\text{-value} < 0.0001$; ****, $+0.0001 < p\text{-value} < 0.00001$

cells (CHO) (Supplemental_Table_M1 and Supplemental_Fig_S2 and S3). Our analysis shows that in most cases chromosome 4 and chromosome 10 are indistinguishable even by using primers already tested in other publications [15, 17, 18, 38–40]. Our qPCR analyses (Fig. 1B, C) showed that 4q35 genes are differentially expressed depending on their chromosomal position, confirming previous evidence [6, 41–43]. Specifically, in control cells, the centromeric *SLC25A4*, *FAT1* and *FRG1* genes displayed high levels of expression in basal condition, whereas *FRG2*, *DBE-T* and *D4Z4-T* were barely detectable. Consistent with the expected derepression of the locus associated with reduced *D4Z4* copy number, *FRG2*, *DBE-T* and *D4Z4-T* transcripts were significantly upregulated in FSHD1 cells (Fig. 1B and C). In contrast, *SLC25A4* and *FRG1* transcripts were found at comparable levels in both control and FSHD cells. Therefore, the loss of *D4Z4* satellites in the FSHD patients' cells correlated with an altered regulation of the telomeric transcripts.

We could not reliably quantify the *DUX4-FL* transcript via qPCR with commonly used primers [17, 18, 38, 39] due to the very low amount of the detected amplicon (Ct values over 35) and because of the presence of multiple peaks in the melting curve analysis of the PCR products (Supplemental_Fig_S1). Indeed, it has been reported that *DUX4-FL* transcripts are detectable only in a small percentage of FSHD-derived myoblasts (1 per 1000 cells) [21] and in cell lines only by using multi-step nested PCR [15, 21, 44, 45]. To perform an unbiased transcriptional analysis of the 4q35 locus, we deliberately avoided pre-amplification steps to quantify *DUX4-FL* transcripts.

The results presented above suggest that genes located at different distances from the *D4Z4* array might undergo a distinct transcriptional regulation. To verify this possibility, we investigated the chromatin features of the 4q35 region by chromatin immunoprecipitation (ChIP) experiments in HPMS and HTC cells using antibodies raised against histones tail modifications associated with transcriptional regulation: AcH3, AcH4 and H3K4me3, H3K9me3 and H3K27me3 (Fig. 1D, E, values in Supplemental_Table1). We detected three classes of modification patterns. As shown in Fig. 1, within the centromeric region of 4q35 active chromatin marks were found at the *SLC25A4* and *FAT1* promoter regions, in both primary cell types, with enrichment of AcH3, AcH4 and H3K4me3, and low levels of H3K9me3 and H3K27me3. At the *FRG1* and *FRG2* promoters, both repressing and activating marks were observed. This “bivalent” pattern of histone modification is characteristic of “poised” promoters that are inactive but able to respond to external stimuli

[46–48]. Specifically, we detected the enriched levels of AcH4 and H3K9me3 at the *FRG1* promoter in both cell types, at comparable levels in control and DRA-bearing cells. At the *FRG2* promoter, we observed comparable levels of AcH4 in control and FSHD-derived cells, whereas H3K9me3 enrichment was significantly more elevated in FSHD-derived myoblasts compared to control cells. A poised chromatin modification pattern at the *FRG2* promoter is a conserved feature in multiple cell types, as confirmed by chromatin state segmentation by HMM from studies by ENCODE/Broad [49] (Supplemental_Fig_S4).

Since the *FRG2* gene is present in multiple copies within the human genome, and their transcriptional activity remains unclear, we aimed to rule out the possibility that the poised chromatin status observed could be due to our primers amplifying different promoters. These promoters might have distinct epigenetic features reflecting their varied transcriptional states. To further validate the specificity of primers amplifying the *FRG2* promoter at 4q35, we designed new oligonucleotides to specifically amplify promoters of different *FRG2* paralogs. As shown in Supplemental_Fig_S5, *FRG2A* (4q35) and *FRG2EP* (chr20) primers indicated a poised promoter state in ChIP experiments on human control myoblasts, while primers targeting *FRG2C* (chr3) and *FRG2FP* (chr3) revealed the presence of an active and repressed promoter, respectively. These findings show the distinct epigenetic patterns at the promoter region of *FRG2* paralogs.

At the *D4Z4* repeat array, we detected enrichment of H3K9me3 associated with low levels of the other chromatin marks analyzed (Fig. 1D, E). A similar epigenetic pattern was found at the gene desert region *LILA5* (Supplemental_Fig_S6), as expected in heterochromatic regions. These epigenetic patterns were displayed likewise in samples from healthy individuals and from FSHD patients with *D4Z4*-deleted alleles (DRAs) with the exception of H3K9me3 whose levels were significantly increased at the *FRG2* promoter and at *D4Z4* in primary cells carrying a DRA [17, 38]. This might seem to conflict with our observation that both *FRG2* and *D4Z4-T* were derepressed in cells carrying a DRA (Fig. 1B and Supplemental_Table_M3). However, these data are consistent with previous results in cells from patients with ICF (immunodeficiency, centromeric region instability, facial anomalies syndrome), in which *D4Z4* transcription is detected in spite of retention of H3K9me3 [50]. In sum, 4q35 contains three subdomains with euchromatic, poised and heterochromatic features, arrayed in a centromere-to-telomere order.

The *FRG2* promoter is activated by inhibition of histone acetylation or PARP1, in a manner regulated by D4Z4 repeat length

The detection of *FRG2* and D4Z4 transcription in FSHD-derived cells despite the enrichment of heterochromatin-associated histone marks at their promoters suggested complex modes of regulation. The different epigenetic patterns observed at promoters of genes involved in FSHD suggest that different mechanisms might intervene in their differential expression. This possibility could have clinical relevance, as the expression levels of 4q35 genes might be regulated by specific stimuli or environmental factors that modulate their transcriptional activity. To investigate the responsiveness of 4q35 gene expression to chromatin modifications, we pharmacologically inhibited different classes of chromatin-modifying enzymes in both HTC and HPMs (Fig. 2) and measured the RNA levels by RT-qPCR. We treated cells with trichostatin A (TSA), an inhibitor of class I, II, IV, histone deacetylases (HDACs) [51], nicotinamide (NAM) [52], an inhibitor of class III HDACs (sirtuins), or PJ34, an inhibitor of Poly (ADP-ribose) polymerase-1 (PARP1) [53–55]. These treatments were performed either in the presence or absence of 5-Aza-dC (Aza), an inhibitor of DNA methylation [51]. After these treatments, minor changes in expression of *SLC25A4*, *FAT1* and *FRG1* (Fig. 2A–C and G–I) were observed.

In contrast, strong transcriptional induction of *FRG2* was observed upon TSA and PJ34 treatments (Fig. 2D and J, note the y-axis scale). The effects of both these compounds were enhanced by 5-aza-dC, indicating that DNA methylation contributes to *FRG2* silencing. Like the centromere-proximal genes, transcription of *DBE* and D4Z4-T transcripts was not induced by the selected compounds (Fig. 2E, F and K, L). We conclude that the *FRG2* promoter is particularly sensitive to local chromatin modifications.

To determine how TSA-induced transcriptional changes correlated with altered histone modifications, we performed ChIP experiments (Supplemental_Fig_S7, data in Supplemental_Table_M3). In both control and DRA-bearing cells, TSA led to a general increase of open chromatin marks (acetylated H3/H4 and H3K4me3) at 4q35 genes. In particular, and consistent with its transcriptional upregulation, we observed increased H3 and H4 acetylation at the poised *FRG2* promoter in HPMs and HTCs bearing one DRA allele (Supplemental_Fig_S7). Together, our data indicate that histone acetylation and D4Z4 repeat length both contribute to the robust inducibility of the *FRG2* promoter.

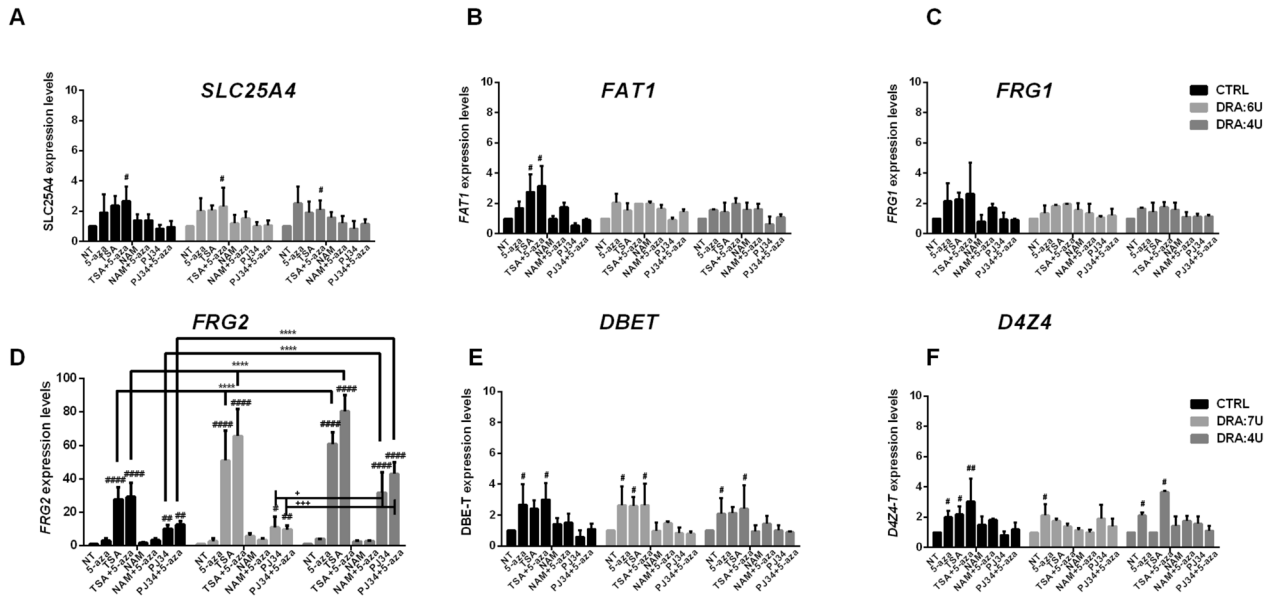
Transcription of *FRG2* and D4Z4 macrosatellite sequences is induced by genotoxic agents

The treatments with epigenetic drugs revealed a different responsiveness of 4q35 genes. In particular, we discovered that PJ34, a PARP1 inhibitor, has a relevant effect on the expression of *FRG2* which seemed to be the most responsive to treatments. PARP1 is a DNA-dependent ADP-Ribose transferase with ADP-ribosylation activity that is triggered by DNA breaks and non-B DNA structures to mediate their resolution and its inhibition results in an accumulation of unresolved R-loops which promotes genomic instability. We thus asked whether 4q35 transcription might be affected by environmental perturbations causing genomic instability. To test this possibility, we treated primary cells with the genotoxic agents cisplatin (CIS) [56], etoposide (ETO) [57] and doxorubicin (DOXO) [12, 58] (Fig. 3 and Supplemental_Fig_S8). As shown in Fig. 3, the centromeric genes (*SLC25A4*, *FAT1* and *FRG1*) were mildly repressed upon genotoxic injury.

To further substantiate this observation, we investigated the expression, upon genotoxic injury, of eight additional coding genes located in the 4q35 region, which have previously been reported to be deregulated in FSHD samples [41, 59, 60]. As reported in Supplemental_Fig_S8, these genes are expressed in HPMs, following a gradient from the most centromeric to the most telomeric positions. None of the genes showed significantly a different expression between FSHD patients and controls, nor did they respond to doxorubicin treatment. In contrast, the expression of *FRG2*, *DUX4-T* and *DBE-T* significantly increased in the presence of all these compounds, in both control and FSHD-derived cells. Additionally, upon treatment with genotoxic agents the amounts of 4q35 telomeric transcripts *FRG2*, *DBE-T* and *D4Z4-T* were significantly increased in HPMs and HTCs bearing a DRA in comparison with cells bearing normal sized D4Z4 alleles. Based on these results, we conclude that RNA levels from telomeric 4q35 genes are induced by genotoxic agents, and the magnitude of this effect is increased by the presence of shortened D4Z4 arrays.

To investigate whether the 4q35 chromatin is affected by DNA damage, we evaluated the amounts of histone isoforms that serve as DNA damage indicators: phosphorylated H2AX (γ H2AX), which appears at DNA double-strand breaks, and macroH2A1.1, which is recruited to sites of DNA damage-induced PARP1 activation [58, 61, 62] (Fig. 3G, H, values in Supplemental_Table2). At *FRG2*, we detected low levels of both these histones in the absence of DOXO treatment. At the D4Z4 locus, macroH2A.1 and γ H2AX are present at very low levels in untreated control cells and significantly increase upon doxorubicin (DOXO)

Human Primary Myoblasts (HPMs)



Human Trophoblast cells (HTCs)

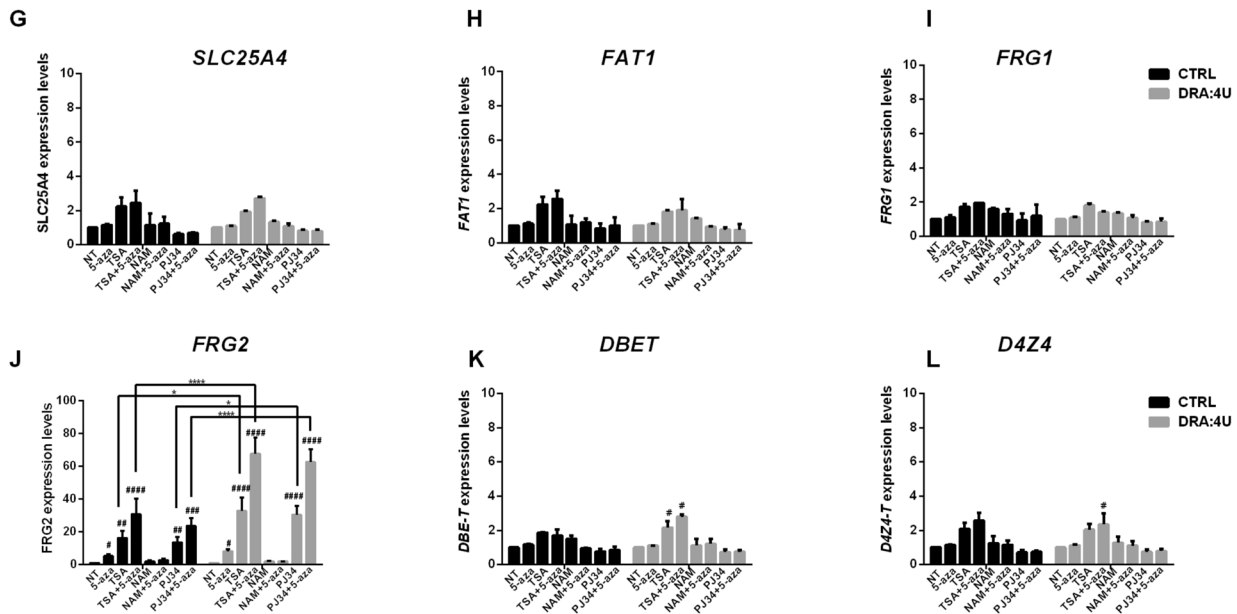


Fig. 2 4q35 gene expression is affected by epigenetic drugs depending on 4q allele size. Expression data of 4q35 genes in human primary myoblasts (HPMs) (A–F) and in human trophoblasts cells (HTCs) (G–L) carry a normal sized allele (CTRL (> 10U)) or D4Z4 reduced alleles (DRA:7U and DRA:4U). Cells were treated or not treated with the indicated compounds: 5-Aza-2'-deoxycytidine (5-Aza-dC), trichostatin A (TSA), nicotinamide (NAM), PARP inhibitor (PJ34). SLC25A4 (A,G), FAT1 (B,H), FRG1 (C,I), FRG2 (D,J), DBE-T (E,K) and D4Z4-T (F,L) RNAs were measured by RT-qPCR and normalized over the *RPLP0* reference gene. The values of the CTRL samples (n = 3) and FSHD DRA:4U (n = 2) were averaged. Experiments were done in triplicate, and the results were analyzed using two-way ANOVA tests to perform multiple comparisons. Hash-tags (#) indicate the statistical significance of data from treated samples compared to untreated samples (NT) in each group. Asterisks (*) indicate statistical significance of data from treated cells carrying DRA compared to the same treatment in control cells. Plus signs (+) indicate statistical significance of data from DRA:7U compared to DRA:4U cells. P value ranges are as follows: *, #, + 0.05 < p-value < 0.01; **, ##, ++ 0.01 < p-value < 0.001; ***, ###, +++ 0.001 < p-value < 0.0001; ****, ####, ++++ p-value < 0.0001

treatment. In FSHD cells, macroH2A.1 and γ H2AX are instead already enriched in untreated cells and increase further significantly following DOXO treatment (Fig. 3H). These observations suggest distinct chromatin architectures at 4q35 alleles that contain a DRA, in which the macrosatellite deletion renders the locus more accessible to DNA damaging agents and/or to DNA damage response factors.

We also evaluated histone modifications at the 4q35 genes in response to exogenous stresses (Fig. 3I–N and Supplemental_Fig_S9, values in Supplemental_Tables2 and 4). Our analysis revealed that the DOXO-mediated increase of *FRG2*, *DBE-T* and *D4Z4-T* transcripts was not associated with local enrichment of histone acetylation or other transcription-associated histone modifications (Fig. 3I–K and Supplemental_Fig_S9A–B). Instead, a significant increase of H3K9me3 at *D4Z4* loci (p -values < 0.001 and < 0.01) was observed. Furthermore, H3K9me3 levels became significantly greater in cells bearing a DRA than in control cells, both at the *FRG2* promoter (p -value < 0.001) and the *D4Z4* array (p -value < 0.05). Treatment with PARP inhibitor PJ34 also induced a robust increase in H3me3K9 (p -value < 0.001) at *FRG2* promoter and *D4Z4* in DRA cells (Fig. 3L–N and Supplemental_Fig_S9C–D). Therefore, the increased RNA levels observed at the 4q35 telomeric genes upon genotoxic stress or PARP inhibition are paradoxically accompanied by increased H3K9 methylation.

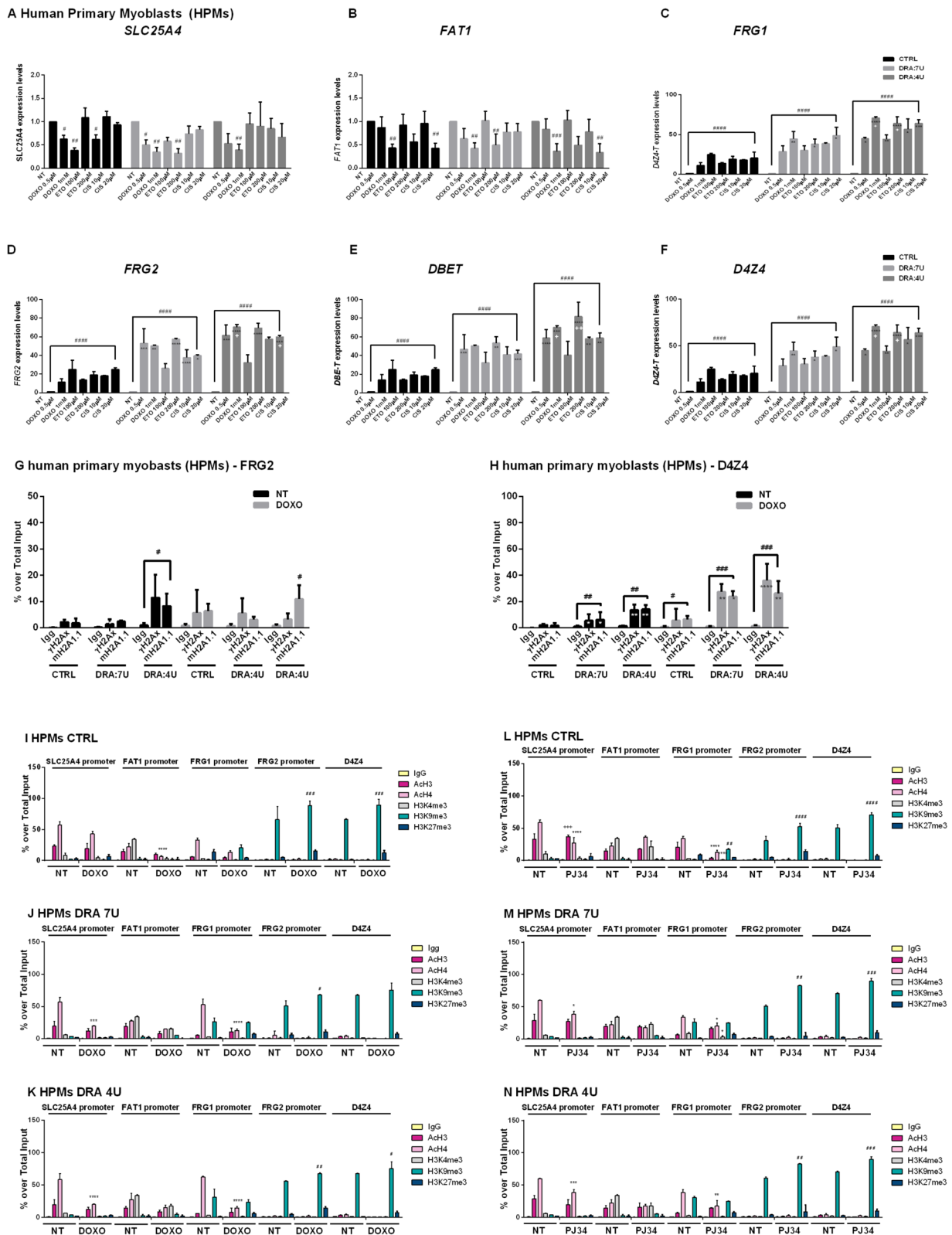
Data from CTRL samples ($n=3$) and FSHD DRA:4U ($n=2$) were averaged. ANOVA statistical test with multiple comparison was performed ($*0.05 < p$ -value < 0.01 ; $**0.01 < p$ -value < 0.001 ; $***0.001 < p$ -value < 0.0001 ; $****p$ -value < 0.0001). Different symbols: * (asterisk), + sign (plus sign) and # (hashtag) refer to different antibodies used in ChIP experiments (* = AcH4; + = AcH3; # = H3K9me3 to show the statistical significance of data obtained in treated cells in respect to the same in not treated cells).

The 4q35 region lacks responsiveness to external noxa in myotubes.

It has been shown that 4q35 genes are differentially expressed in skeletal muscle cells undergoing differentiation [39, 63–65]. To determine whether differences exist in the regulation of 4q35 genes in differentiated cells, we induced myogenic differentiation in both control and FSHD myoblasts. First, purity of myoblast cultures was evaluated by immunostaining for desmin (Supplemental_Fig_S10A–D). Then, their differentiation capacity was assessed eight days after the induction of differentiation (Supplemental_Fig_S10E–U). As shown in Supplemental_Fig_S10T,U, we observed an impairment of differentiation ability in FSHD myoblasts, showing a fusion index percentage of 45–50%, compared with the 70% observed in control cells, and a differentiation index of 55–60% compared with the 70–75% of control cells. The analysis of 4q35 transcripts genes following myoblast differentiation into myotubes revealed a significant increase in *FRG1* transcript (Supplemental_Fig_S11A), along with the appearance of *DUX4-FL* transcript in FSHD myotubes and a strong increase in *PDLIM3* expression in both patients and controls confirming previous results (PMID: 9334352, PMID 10063829) (Supplemental_Fig_S11F) [66, 67]. *D4Z4-T* and *DBE-T* transcripts were also slightly increased in FSHD myotubes while *FRG2* levels remained unchanged, consistent with previous findings [68] (Supplemental_Fig_S11A). To determine whether the stress responsiveness of telomeric genes persists after cell proliferation ceases, we measured the expression levels of *FRG1*, *D4Z4-T*, *DBE-T* and *FRG2* in myotubes treated with genotoxic agents (Supplemental_Fig_S11C–E). Additionally, we evaluated the responsiveness of centromeric coding genes to DOXO (Supplemental_Fig_S11F). Our results indicated that, compared to myoblasts, none of the tested regions exhibited transcriptional induction following DNA damage. This suggests that telomeric genes are responsive to stress during the proliferative stage, highlighting the unique gene regulatory properties of myoblasts compared to myotubes. This lack of response in myotubes is likely due to a known reduced

(See figure on next page.)

Fig. 3 4q35 genes show different responsiveness to DNA damage depending on *D4Z4* size and subtelomeric localization. Control HPMs, DRA:7U HPMs and DRA:4U HPMs were untreated or treated with genotoxic drugs: doxorubicin (DOXO), etoposide (ETO) and cisplatin (CIS), at the reported concentrations. **A–F** Expression of *SLC25A4* (**A**), *FAT1* (**B**), *FRG1* (**C**), *FRG2* (**D**), *DBE-T* (**E**) and *D4Z4-T* (**F**) was evaluated 24 h after treatments and normalized over *RPLP0*. The values of the CTRL samples ($n=3$) and FSHD DRA:4U ($n=2$) were averaged. Error bars represent standard deviation values for three independent replicates. Hashtags refer to statistical significance of treated samples in respect to not treated samples (NT). Asterisks refer to statistical significance of treated cells carrying DRA in respect to the same treatment in control cells in each group. Plus signs refer to statistical significance of 4U DRA compared to 7U DRA. G–H) ChIP in HPMs treated or not with doxorubicin. Antibodies directed to γ H2Ax and macroH2A1.1 (mH2A1.1) were used, followed by qPCR amplification of *FRG2* (G) and *D4Z4* (H). I–N) ChIP conducted in control and DRA HPMs that were untreated or treated with doxorubicin (I–K) or PJ34 (L–M). Antibodies directed to H3K4me3, H3K9me3, H3K27me3 and pan-acetylated Histone 3 and 4 (AcH3 and AcH4) were used, followed by qPCR amplification using primers described in Fig. 1A



efficacy of the DNA damaging drugs in differentiated cells [69]. We also conducted ChIP experiments in myotubes derived from our myoblast samples to explore potential differences in 4q35 genes regulation after differentiation (Supplemental_Fig_S12). After ChIP, we amplified eight different regions across the 4q35: *SLC25A4* promoter, *FAT1* promoter, *FRG1* promoter, *FRG2* promoter, *DBE-T* (NDE region), *D4Z4* (DBE region) and *D4Z4* Q-PCR, by using primer sets detailed in Supplemental_Table_M1. ChIP results were normalized over Pan Histone H3-precipitated material to account for potential variability in histone loading caused by different stages of cell differentiation. Our results confirmed the elevated levels of H3K9me3 histone mark in FSHD myotubes compared to control myotubes, as observed through the amplification of two different regions at *D4Z4* (DBE and Q-PCR) regions. Consistent with previously reported data [18], we detected the enrichment of the H3K27me3 at the *DBE-T* (NDE) region in both myoblasts and myotubes from control and FSHD-derived cells. Consistent with the expression results, the ChIP analysis conducted after DOXO treatment (Supplemental_Fig_S12C,D) showed a global loss of histone marks at the 4q35 region. Notably, this reduction was accompanied by a significant decrease in histone acetylation and H3K4me3 methylation, which occurred preferentially at the more centromeric genes.

Transcripts from telomeric 4q35 genes are posttranscriptionally stabilized upon DNA damage

We observed that *FRG2* transcript levels were induced by TSA treatment and this induction was accompanied by increased histone H3/H4 acetylation in cells carrying *DRA* alleles (Fig. 2). In contrast, the elevated levels of *FRG2*, *DBE-T* and *D4Z4* transcripts following genotoxic injury were not associated with histone modifications typical of transcriptional activation. Instead, we observed an increase in H3K9me3 levels (Fig. 3). These observations, inconsistent with typical gene activation scenarios, prompted us to investigate whether this increase could be explained by posttranscriptional stabilization of telomeric 4q35 transcripts. To test this possibility, we treated control or FSHD HTC cells with actinomycin D (ActD), at concentration sufficient to inhibit transcription by both RNA polymerase I and II [70] and then evaluated the stability of 4q35 transcripts over time. Experiments were performed with ActD alone or in the presence of DOXO (Fig. 4). We also amplified 5S rRNA, transcribed by RNA polymerase III, and observed that its levels remained stable, serving as a control for RNA normalization (Supplemental_Fig_S13). Notably, the expected increase in *FRG2*, *DBE-T* and *D4Z4-T* transcript levels in the presence of DOXO was also observed when transcription was inhibited by ActD treatment (Fig. 4D–F). Following

the hypothesis that the increased RNA levels were due to posttranscriptional stabilization, we quantified the half-lives of these three telomere-proximal RNA species (Fig. 4A) and found that these RNAs have extended half-lives in cells carrying *DRA* alleles. We conclude that the major regulatory event for the 4q35 telomere-proximal transcripts upon genotoxic stress is posttranscriptional stabilization.

These findings raised the question if this phenomenon is characteristic of the 4q35 telomeric transcripts. To verify this hypothesis, we evaluated the effect of transcriptional inhibition using actinomycin D (ActD) and doxorubicin (DOXO) also on U2 transcripts (from the U2 macrosatellite; CHM13/chr17:44,114,587-44,167,305) as shown in Supplemental_Fig_S13. Interestingly, these transcripts were slightly induced only by DOXO plus ActD, but not with DOXO alone, suggesting the presence of an alternative mechanism and highlighting new possibilities for exploring how repetitive elements are differentially regulated in response to DNA damage.

Transcripts from 4q35 telomeric genes are chromatin-associated

The observation that *FRG2*, *DBE-T* and *D4Z4-T* transcript levels are affected by the same stimuli raises the question of whether these RNAs have additional commonalities. Since repetitive element RNAs often function as components of chromatin fibers [71], we performed RNA fractionation experiments in primary control or FSHD-derived myoblasts (Fig. 5A, B). In both cell samples, *FRG2* and *D4Z4-T* RNAs were enriched in the chromatin-associated fraction and behaved similarly to the previously characterized chromatin-associated transcripts *lncDBE-T* and *TERRA* [18, 72]. As control or the fractionation, we confirmed that the *lncRNA NEAT1* was prevalently found in the nuclear fraction, and the protein-coding mRNA *GAPDH* was preferentially enriched in the cytoplasm.

The chromatin association of the *FRG2*, *DBE-T* and *D4Z4-T* transcripts was confirmed by chromatin-RNA immunoprecipitation (ChRIP) [73] conducted in primary myoblasts from control and FSHD subjects using H3K4me3, H3K9me3 and H3K27me3-specific antibodies (Fig. 5C). *FRG2*, *DBE-T* and *D4Z4-T* transcripts were selectively and significantly enriched in H3K9me3 and H3K27me3-marked chromatin. As a control for the selectivity of our analysis, we confirmed that *lncRNA NEAT1*, known to be associated with actively transcribed genes, was enriched in H3K4me3-marked but not H3K9me3 or H3K27me3-marked chromatin [74].

Together, our findings reveal that the telomere-proximal 4q35 genes share important regulatory features: their transcript levels are induced by genotoxic stress

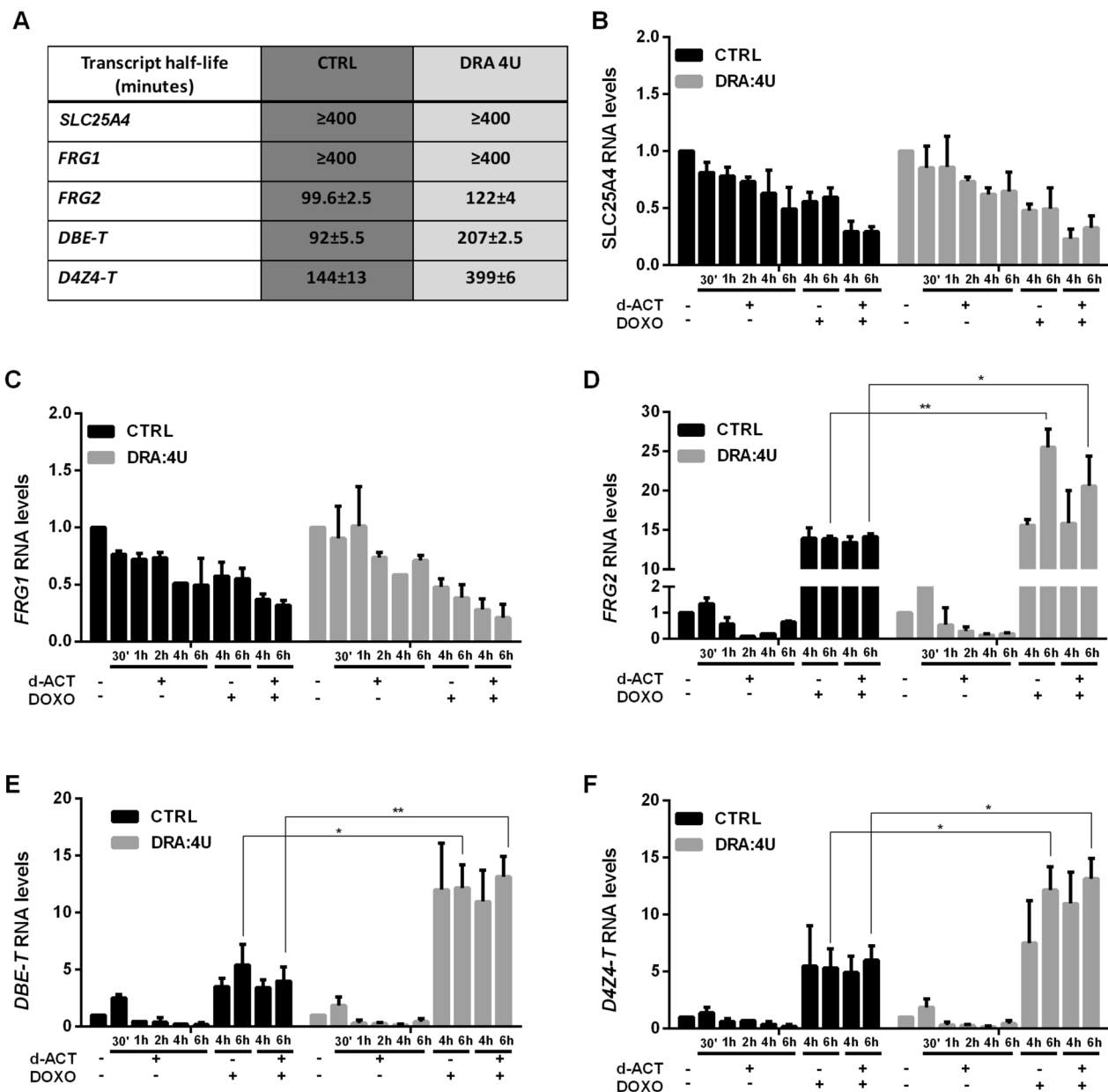


Fig. 4 4q35 telomeric transcripts are stabilized upon DNA damage and transcriptional inhibition dependently on D4Z4 size reduction. **A** Table reports the half-life of 4q35 transcripts measured after actinomycin D (ActD) treatment in CTRL ($n=2$) and DRA:4U ($n=2$) HPMs. **B–F** Cells were treated with ActD for the indicated times (30', 1 h, 2 h, 4 h and 6 h) in the presence or absence of DOXO, and the levels of 4q35 gene transcripts were evaluated by qPCR. The half-life of each RNA was calculated as the time needed to reduce the transcript level to half (50%) of its initial abundance at time 0. Data shown are means \pm s.e.m. of three replicates. The values of the CTRL samples ($n=2$) and FSHD DRA:4U ($n=2$) were averaged

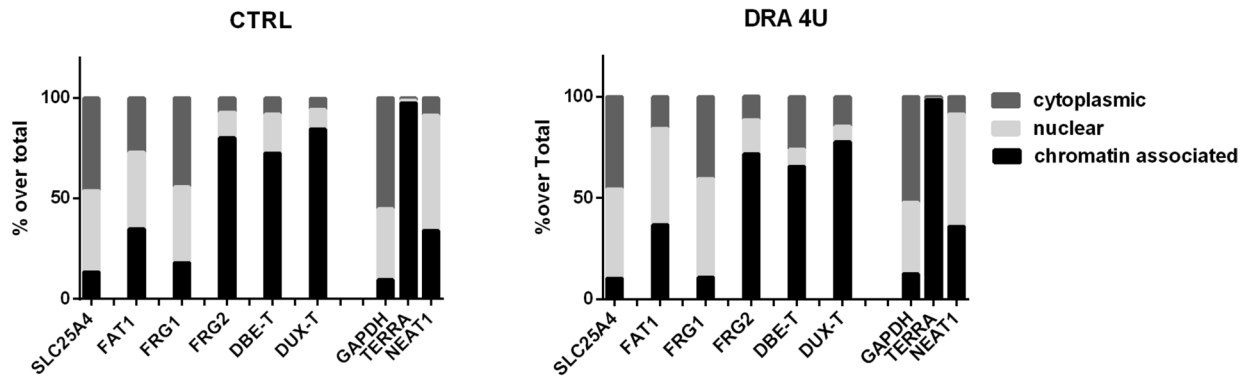
via posttranscriptional stabilization, and these RNAs are all chromatin-associated (Fig. 6). Furthermore, the regulation of these telomeric transcripts is affected by the size of the D4Z4 subtelomeric array (Figs. 2 and 3). Therefore, the regulatory potential of this locus is expected to be variable in the human population.

Discussion

Regulation of telomeric 4q35 transcripts provides insights for understanding clinical variability and low penetrance in FSHD

Our study demonstrates that the 4q35 region is subdivided into discrete domains, each with characteristic

A HPMs-human primary myoblasts B



C

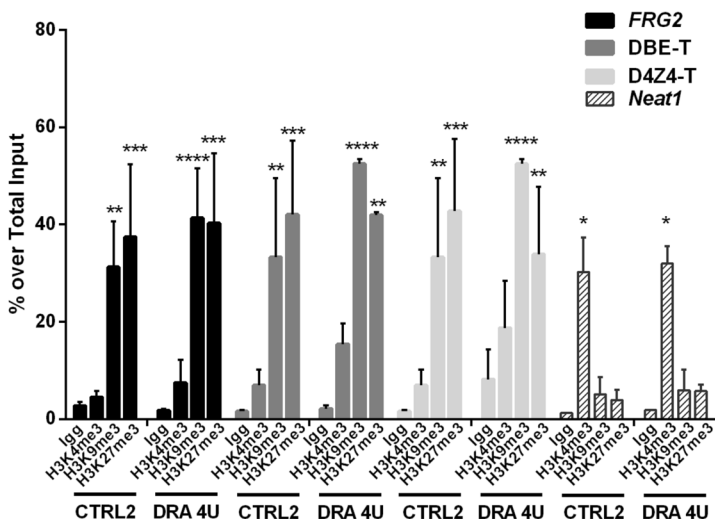


Fig. 5 4q35 genes regulation upon different stimuli reflects architectural and epigenetic patterns. **A, B** RNA fractionation experiments were conducted in CTRL (A) (n=2) and DRA:4U (n=2) (B) HPMs. Transcripts from the indicated 4q35 genes were measured by qPCR analysis of cytoplasmic, nuclear and chromatin-associated RNA fractions, and the percentage detected in each fraction over total RNA was graphed. GAPDH, TERRA and NEAT1 transcripts were also assessed as positive controls that are most enriched in cytoplasmic, chromatin and nuclear fractions, respectively. **C** Chromatin-RNA Immunoprecipitation (ChRIP) experiment performed in HPMs. Antibodies directed to H3K4me3, H3K9me3, H3K27me3 were used to precipitate RNA from CTRL and DRA:4U cells. Data shown are means \pm s.e.m. of three replicates. * (asterisks) refer to each different antibody used in ChRIP experiment to show the statistical significance of data obtained for each antibody over control IgG

chromatin features associated with distinct gene expression profiles. These discrete domains provide specific properties to the encompassed genes. Further, our results indicate that the telomeric 4q35 genes share peculiar and similar properties, completely different from the rest of the 4q35 region. While the centromeric 4q35 genes are protein-coding, the telomeric transcripts, FRG2, DBE-T and D4Z4-T, are noncoding RNAs, which associate with heterochromatin. We also detected three epigenetic patterns at the 4q35 locus, with centromeric genes displaying active promoters and telomeric genes with repressed chromatin histone marks, whereas FRG1 and FRG2

are characterized by the presence of a poised chromatin domain, which defines the boundaries of these two groups of genes at 4q35.

It is important to note that the myoblasts used in our study do not express DUX4-FL, in contrast to those analyzed in other reports. As a result, some of the observed differences may stem from intrinsic variations in the epigenetic regulation of the 4q35 region across different cellular contexts. Cells expressing or not expressing DUX4-FL have been shown to exhibit distinct chromatin landscapes at D4Z4, corresponding to permissive and nonpermissive transcriptional states. This distinction is

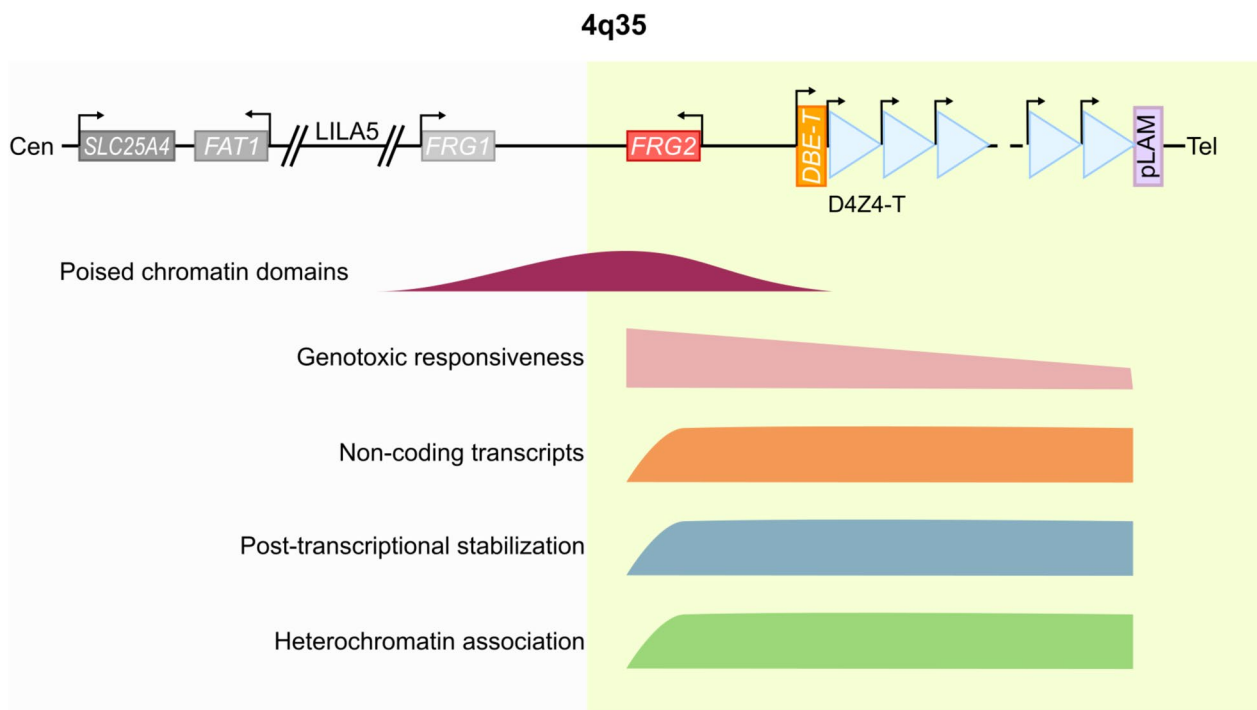


Fig. 6 4q35 genes regulation upon different stimuli reflects architectural and epigenetic patterns. Schematic representation of the 4q35 locus summarizing the key characteristics of its telomeric genes reveals new insights into the functional subdomains within the 4q subtelomere. Our study demonstrates that these regions exhibit distinct chromatin features, which are reflected in their differential responses to external stimuli. Genotoxic injury leads to overexpression along a gradient starting from *FRG2*—where the chromatin is poised—and extending toward the telomere. *FRG2*, *DBE-T* and *D4Z4-T* transcripts share several common features. They are: (i) noncoding RNAs, (ii) stabilized posttranscriptionally upon exposure to genotoxic stress, and (iii) associated with heterochromatin. This transcriptional model applies to both control cells and cells carrying a reduced *D4Z4* allele, with the induction or stabilization of these transcripts inversely correlated with the size of the *D4Z4* repeat array

particularly relevant, as *DUX4-FL* has been implicated in the direct regulation of genes such as *FRG1* and *FRG2*, potentially influencing broader transcriptional programs. This highlights the importance of considering cellular context when investigating 4q35 regulatory dynamics and suggests that multiple, context-dependent mechanisms may contribute to FSHD pathogenesis.

Starting from *FRG2*, these telomeric transcripts are susceptible to different stimuli. At basal conditions, they are barely expressed, but they are abnormally upregulated upon genotoxic treatments, in a manner independent from an active transcriptional process. We discovered that this increase is due to their extended half-life induced by posttranscriptional events. This posttranscriptional stabilization suggests that 4q35-derived telomeric transcripts could be degraded in physiological conditions or in the absence of a DRA. It remains unclear which roles they may play in cellular processes. Interestingly, this responsiveness has been detected in both control and DRA-bearing cells, but the magnitude of upregulation is inversely correlated with the *D4Z4* size. This correlation links the response to drug treatments

with the number of *D4Z4* repeats, offering an element to associate environmental changes (in this case DNA damage) to aberrant amounts of *FRG2*, *DBE-T* and *D4Z4-T* transcripts.

While our data do not support a direct role for *D4Z4* repeat number in modulating posttranscriptional mechanisms, we propose that this phenomenon may result from a cascade effect triggered by changes in transcriptional regulation. Specifically, these secondary effects might arise from alterations in the abundance or structure of primary transcripts, or via indirect mechanisms such as the activity of RNA-binding proteins or noncoding RNAs that interact with these transcripts.

Intriguingly, the transcripts increase upon drug treatments is not present in terminally differentiated myotubes, suggesting that subtelomere responsiveness is a mechanism present only in proliferating cells (HPMs, HTC), and thus could be influenced by or required during active proliferative stages.

As components of the chromatin fiber, these RNAs could favor regulatory *cis* chromatin interactions at 4q35 [18], as well as *trans* interactions with other repetitive

elements interspersed across the human genome. Furthermore, as D4Z4-like sequences are highly polymorphic and account for several hundreds of Kbs in each individual genome [30], further studies will be required to determine the extent of D4Z4 and D4Z4-like RNA molecules produced, how these differ in different individuals, and how their interaction patterns impact genome function. Overall, FSHD offers a valuable natural model to understand the complex interplay between tandemly arrayed repeats and their function in genomic architecture and phenotypic heterogeneity. The development of long read DNA and RNA sequencing technologies offers unprecedented possibilities for in-depth molecular phenotyping and for the interpretation of results in a multi-dimensional perspective.

A role for DNA repetitive elements in personalized medicine

Our study reports an additional element to define the dynamics of the FSHD locus at 4q35. The most telomeric part of the 4q35 region presents peculiar features that are influenced by the number of D4Z4 repeats. Our experiments demonstrate that genotoxic treatments induce chromatin modifications at the 4q35 subtelomere that could generate an abnormal quantity of FRG2, DBE-T and D4Z4-T transcripts in cells with a DRA. One of the current challenges in molecular medicine is to understand how DNA variations in noncoding sequences translate into phenotypic variability among individuals. Repetitive DNA elements represent 56–69% of the human genome [1, 2, 75–77]. Although macrosatellite repeats have been less well studied than many repeat classes, there is increasing evidence for a strong correlation between macrosatellite copy number, epigenetic modifications and local gene expression [78–80]. Thus, macrosatellites provide an example of repeat-induced gene silencing as a mechanism of gene regulation in humans.

Our work demonstrates that the D4Z4 macrosatellite array alters transcriptional responses to drugs at nearby genes, and that the number of repetitive elements modulates these changes. It is thus possible that what we observe at the 4q35 D4Z4 locus may occur at other macrosatellites interspersed within the genome. These sequences are highly polymorphic between individuals and heritable. Therefore, correlations between macrosatellite composition, size and their responsiveness to drugs could facilitate the understanding of how a person's repetitive DNA profile contributes to disease susceptibility and could increase our ability to predict the results of specific medical treatments. In this manner, better knowledge of the biological roles of repeats may offer substantial tools for personalized medicine.

Material and methods

Cell culture and drugs treatment

Primary trophoblast cell cultures were established immediately and after chorionic villus sampling (HTCs), and cells were grown in Ham's F10 medium (Corning) plus L-glutamine, 20% FBS and 1% penicillin/streptomycin. Human chromosome hybrids (CHO/Hyb) were obtained from the Coriell Institute for Medical Research. Cells were maintained following manufacturer's instructions. Healthy and FSHD-derived human primary myoblasts (HPMs) were cultured in DMEM, added with 20% FBS, 1% L-glutamine, 1% penicillin/streptomycin, 2 ng/mL epidermal growth factor (EGF) and 25 ng/mL of fibroblast growth factor (FGF). Both cell lines and primary cells were grown on T75 flasks in a humidified atmosphere at 37 °C with 6% CO₂. Cells were treated with TSA (Sigma; T8552), PJ34 (Sigma; 528,150) 5-aza-cytidine (Sigma; A3656); NAM (Sigma; N0636); doxorubicin (Sigma; D1515); actinomycin D 1 µg/ml (Sigma; SBR00013). Treatments with 1 µg/mL actinomycin D were performed for 1 h prior to the addition of doxorubicin (DOXO). The DOXO treatment was subsequently applied for either 3 or 5 h, depending on the experimental condition.

Myoblasts differentiation

Human primary myoblasts (HPMs) from CTRL and FSHD patients were induced to differentiate between passages P3 and P5. To induce differentiation, myoblasts were plated at a confluence of 15 000 cells/cm² and, 24 h after seeding, growth medium was replaced by differentiation media composed by DMEM supplemented with 10% FBS, 1% glutamine and 1% penicillin–streptomycin, without the addition of EGF and FGF. Medium was changed every 2–3 days. The resulting myotube cultures were used for analysis at day 8 (D8) of myogenic differentiation, after assessing their complete differentiation by calculating the fusion index (number of nuclei inside myotubes positive for sarcomeric myosin-staining containing at least three nuclei/total number of nuclei) and differentiation index (number of nuclei inside myotubes positive for sarcomeric myosin-staining/total number of nuclei; and by RT-qPCR amplification of muscle-specific molecular markers (MyoD and Myogenin).

Immunofluorescence

Immunofluorescence assays were performed to assess the presence of muscular cells and myogenic differentiation. Briefly, human primary myoblasts (HPMs) and myotubes were fixed with 3% paraformaldehyde (PFA) in PBS, for 12 min at room temperature, and permeabilized with 0.5% Triton X-100 in PBS. Slides were incubated

in blocking solution (1% BSA in PBS) for 15 min, and then with primary antibodies (anti-Desmin (Dako M0760) diluted 1:50 and myosin heavy chain (MF20, DSHB#AB_2147781) diluted 1:100) in blocking solution over night at 4°. After washes in PBS, cells were incubated with the secondary antibody (Invitrogen A11001, diluted 1:100) in blocking solution, for 1 h at room temperature. Slides were mounted by using the ProLong™ Glass Antifade Mountant with NucBlue (Invitrogen™, cat #P36981). Images were acquired by using the EVOS M5000 microscope equipped with a 10X or 20X lens.

RNA extraction and real-time quantitative RT-PCR (qRT-PCR)

Total cellular RNA was obtained using a PureLink RNA Mini Kit (Thermo Fisher Scientific cat #12183018A) according to the manufacturer's instructions. DNase digestion and cDNA synthesis was performed by using Maxima H-cDNA Synthesis Master Mix, with dsDNase (Thermo Fisher M1682). Specific mRNA expression was assessed by qRT-PCR (iTaQ Universal SYBR® Green Supermix, BIORAD#1725120 in a CFX connect Real-Time Machine BIORAD) using primers listed in Supplemental_Table_M1, normalized over RPLP0 housekeeping mRNA.

Statistical analyses

All data presented in figures were performed at least in triplicate and expressed as means ± SEM. When making multiple statistical comparisons, one-way ANOVA with Tukey or Dunnett's post hoc tests was used for normally distributed data. All analyses were conducted using Prism software (GraphPad Software Inc.).

ChIP and real-time quantitative RT-PCR (qRT-PCR).

Chromatin immunoprecipitation (ChIP) assays were performed both in cell lines and in primary cells as described earlier [81] using specific antibodies as listed in Supplemental_Table_M2. Immunoprecipitates from at least three independent cell samples were analyzed by quantitative real-time PCR (qPCR) as described above. Enrichment of amplified DNA sequences (primers listed in Supplemental_Table_M1) in immunoprecipitates was calculated as the ratio between the DNA amount in immunoprecipitation samples and that in the total input chromatin.

RNA fractionation

Control and FSHD-derived myoblasts cell pellets (1 million of cells) were lysed with 175 µl of cold cytoRNA solution (50 mM Tris HCl pH 8.0; 140 mM NaCl; 1.5 mM MgCl₂; 0,5% NP-40; 2 mM Vanadyl Ribonucleoside Complex; Sigma) and incubated 5' in ice. Cell suspension was

centrifuged at 4 °C and 300 g for 2' and the supernatant, corresponding to the cytoplasmic fraction, was transferred into a new tube and stored in ice. The pellet containing nuclei were extracted with 175 µl of cold nucRNA solution (50 mM Tris HCl pH 8.0; 500 mM NaCl; 1.5 mM MgCl₂; 0,5% NP-40; 2 mM Vanadyl Ribonucleoside Complex) and incubated 5' on ice. The suspension was centrifuged at 4 °C and 16,360 g for 2' and the supernatant, corresponding to the nuclear-soluble fraction, was transferred into a new tube and stored in ice. The remaining pellet was collected as the chromatin-associated fraction. Total RNA from the cytoplasmic and nuclear fractions was extracted by using PureLink RNA MiniKit (Invitrogen) following the manufacturer's instructions for the RNA extraction from aqueous solutions. The pellet containing the chromatin-associated fraction was extracted with the standard procedure described above for RNA extraction.

Chromatin-RNA precipitation (ChRIP)

Chromatin-RNA immunoprecipitation (ChRIP) was performed as previously described [73] using anti-H3K4me3, H3K9me3 H3K27me3 antibodies as reported in Supplemental_Table_M2. 3 × 10⁶ HPM cells were used for each IP. RNA was extracted and qPCR performed as described above. Ten percent input was used to calculate the percentage of transcript bound to chromatin compared to the negative control IgG.

Supplementary Information

The online version contains supplementary material available at <https://doi.org/10.1186/s13148-025-01881-5>.

Supplementary file 1 SF1 Expression analysis of DUX4-T and DUX4-FL. A) Schematic representation of the last D4Z4 unit, the adjacent pLAM region and the distal exons. The first exon of the DUX4 ORF is contained in each repeat. The pLAM sequence is only present in the DUX4-FL transcript. Primers used for qPCR are indicated in different colors. B–E) qPCR reports of D4Z4-T and DUX4-FL amplification by using the indicated primer pairs, melting curve graphs are visible in the upper part of each graph, melting curve and quantification cycle (C_q) reports are indicated in the table below for human primary myoblasts (HPMs) and human primary fibroblast cells (here HPPFs). For DUX4-FL, we used three different primer sets (DUX4-FL1 in purple, DUX4-FL2 in blue and DUX4-FL3 in green) used in previous works [15,39,40].

Supplementary file 2 SF2 4q35 primers validation and expression analysis in human chromosome hybrids (CHO/Hyb). A–F) 4q35 primer specificity was validated in CHO/hybrids-derived genomic DNA. *FRG2* (A), DBE-T (B), DUX4-Ex1 (C) primer sets amplified both chromosomes 4 and 10; DUX4-FL1 (D) and 2 (E) did not amplify anything, and DUX4-FL3 primers were not specific (F). G–L) Primer specificity was also tested in CHO/hybrid-derived cDNA.

Supplementary file 3 SF3 Primer specificity for the telomeric 4q35 region was evaluated by using CHO/hybrid-derived genomic DNA. *FRG2* promoter CHIP2 (A), DBE-T CHIP (NDE) (B) and D4Z4 CHIP (C) primer sets specifically amplified chromosomes 4 and 10.

Supplementary file 4 SF4 chromatin state segmentation by HMM from ENCODE/Broad; Hg19chr4:190,793,373-191,038,972.

Supplementary file 5 SF5 Validation of *FRG2* paralog-specific primer sets. A) Primer sets amplifying promoters of different *FRG2* paralogs were tested in CHO/hybrid-derived genomic DNA. B) Chromatin immunoprecipitation assay (ChIP) performed in HPMS shows the presence of a poised promoter at *FRG2A* (chr4) and *FRG2EP* (chr20), and an active and repressed promoter at *FRG2C* (chr3) and *FRG2FP* (chr3), respectively.

Supplementary file 6 SF6 Epigenetic status of 4q35-associated gene desert region. Chromatin immunoprecipitation assays (ChIP) conducted in (A) HPMS and HTC (B) carrying a normal sized (CTRL) and reduced (DRA) D4Z4 alleles. Antibodies directed to H3K4me3, H3K9me3, H3K27me3 and pan-acetylated Histone 3 and 4 (Ach3 and Ach4) were used, followed by qPCR amplification using primers described in Supplemental_Table_M1.

Supplementary file 7 SF7. Chromatin immunoprecipitation assays (ChIP) conducted in HTCs carrying a normal sized (CTRL) (A) and reduced (DRA) (B) D4Z4 alleles treated or not with TSA. Antibodies directed to H3K4me3, H3K9me3, H3K27me3 and pan-acetylated Histone 3 and 4 (Ach3 and Ach4) were used, followed by qPCR amplification using primers described in Fig1A. ANOVA statistical test with multiple comparison was performed (*0.05<p value<0.01; ** 0.01<p value<0.001; *** 0.001<p value<0.0001; **** P value<0.0001): \$ (dollar symbol), and * (asterisk). Dollar symbols and asterisks indicate the statistical significance of data obtained in TSA treated cells in respect to the same antibody enrichment in not treated cells. 4q35 regions amplified in qPCR following ChIP are indicated in the upper part of each graph.

Supplementary file 8 SF8 Control HTCs and HTCs bearing 6U D4Z4 array were untreated or treated with genotoxic drugs: doxorubicin (DOXO), etoposide (ETO) and cisplatin (CIS), at the reported concentrations. Expression data of *SLC25A4* (A), *FAT1* (B), *FRG1* (C), *FRG2* (D), *DBE-T* (E) and *D4Z4-T* (F) were evaluated 24h after treatments and normalized over *RPLP0* reference gene levels. Error bars represent standard deviation values for three independent replicates. G) Evaluation of the expression of the centromeric 4q35 genes in HPMS from CTRL and DRA:4U, treated or untreated with doxorubicin (DOXO). The values from CTRL samples (n=2) and DRA:4U samples (n=2) were averaged and normalized over *RPLP0* reference gene. Error bars represent standard deviation values for three independent replicates.

Supplementary file 9 SF9 A–D) Chromatin immunoprecipitation assays (ChIP) conducted in control and DRA HTCs treated or not with doxorubicin (A,B) or PJ34 (C,D). Antibodies directed to H3K4me3, H3K9me3, H3K27me3 and pan-acetylated Histone 3 and 4 (Ach3 and Ach4) were used, followed by qPCR amplification using primers described in Fig1A. ANOVA statistical test with multiple comparison was performed (*0.05<p value<0.01; ** 0.01<p value<0.001; *** 0.001<p value<0.0001; **** P value<0.0001). Different symbols: * (asterisk) and # (hashtag) refer to different antibodies used in ChIP experiments (*=Ach4; #=H3K9me3 to show the statistical significance of data obtained in treated cells in respect to the same in not treated cells). Error bars represent standard deviation values for three independent replicates.

Supplementary file 10 SF10 Differentiation of human primary myoblasts (HPMS) into myotubes. A–D) IF staining with anti-desmin antibody performed in HPMS from CTRLs (A,B) and FSHD patients (C,D). E–J) Visual inspection of differentiating CTRL and FSHD-derived human primary myoblasts by phase contrast microscopy. Human primary myoblasts (E,H) were plated between passages P3 and P5. Cell morphology and cell fusion were evaluated at D4 (F,I) and D8 (G,J) of myogenic differentiation. Images were taken at 10X magnification. K–N). Immunostaining for desmin was performed in differentiated myotubes from CTRLs (K,L) and FSHD patients (M,N). O–R) Immunostaining for sarcomeric myosin heavy chain (MF20) performed after differentiation in both CTRLs and DRA samples, confirming the presence of fused differentiated myotubes. S) Myogenic differentiation was also evaluated by RT-qPCR amplifying muscle-specific markers MyoD and Myogenin. T–U) Fusion Index (T), calculated as the number of nuclei inside MHC-positive syncytia containing at least three nuclei/total nuclei, and the differentiation index (U), calculated as the number of nuclei inside

MHC-positive myotubes/total nuclei, revealed an impairment of myogenic differentiation in FSHD cells compared to CTRLs. Statistical significance was tested by using the unpaired t test (p value***= <0.001).

Supplementary file 11 SF11 A) Basal expression levels of 4q35 genes in human primary myoblasts and myotubes from CTRL (n=2) and FSHD carrying a 4U DRA (n=2). B–E) Evaluation of 4q35 genes expression upon genotoxic treatments, in myoblasts and in myotubes. F) Expression levels of centromeric 4q35 genes in myotubes, treated or not with genotoxic agent doxorubicin (DOXO). The values from CTRL samples (n=2) and DRA:4U samples (n=2) were averaged and normalized over *RPLP0* reference gene. Error bars represent standard deviation values for three independent replicates.

Supplementary file 12 SF12 A–B) Chromatin Immunoprecipitation (ChIP) assays performed in human primary myoblasts (A) and myotubes (B). Antibodies directed to H3K4me3, H3K9me3, H3K27me3 and pan-acetylated Histone 3 (Ach3) were used, followed by qPCR amplification using primers described in Fig1A. Results are reported as a percentage over total histone H3 quantity. ANOVA statistical test with multiple comparison was performed (*0.05<p value<0.01). C–D) Chromatin Immunoprecipitation (ChIP) assays performed in CTRL (C) and DRA-carrier patient (D) myotubes, treated or not with genotoxic agent doxorubicin. Antibodies directed to H3K4me3, H3K9me3, H3K27me3 and pan-acetylated Histone 3 (Ach3) were used, followed by qPCR amplification using primers described in Fig1A. ANOVA statistical test with multiple comparison was performed (**** p value<0.0001). The values from CTRL samples (n=2) and DRA:4U samples (n=2) were averaged.

Supplementary file 13 SF13 Expression of 5s rRNA and U2 macrosatellite-derived transcripts, at basal levels and upon genotoxic agents. U2 and 5srRNA expression was evaluated by RT-qPCR in HPMS

Supplementary file 14

Acknowledgements

We are indebted to all patients and their families for participating in this study. We wish to express our sincere gratitude and recognition to Professor Michael R. Green, who sadly left us too soon, for his significant contributions to our research.

Author contributions

VS and MS contributed to study design, molecular analysis, data collection, data analysis and interpretation, literature search, preparing of figures/tables and manuscript writing. FL performed molecular biology experiments. PDK contributed to data interpretation and manuscript editing. RT contributed to conception and study design, data interpretation, literature search and manuscript writing.

Funding

National Institutes of Health, (R01ns0475840) (to RT), FSHD Global Research Foundation (to RT) and NIH U01 CA260669 (to PDK). Cariplo-Telethon Alliance GJC23060 (to RT). The research, leading to these results, has received funding from the European Union—NextGenerationEU through the Italian Ministry of University and Research under PNRR—M4C2-I1.3 Project PE_00000019 "HEAL ITALIA" to Rossella Tupler CUP E93C22001860006 of University of Modena and Reggio Emilia. The views and opinions expressed are those of the authors only and do not necessarily reflect those of the European Union or the European Commission. Neither the European Union nor the European Commission can be held responsible for them.

Availability of data and material

No datasets were generated or analyzed during the current study.

Declarations

Ethics approval and consent to participate

Not applicable.

Consent for publication

Not applicable.

Competing interests

The authors declare no conflict of interest.

Author details

¹Department of Biomedical, Metabolic and Neural Sciences, University of Modena and Reggio Emilia, Via G. Campi 287, 41125 Modena, Italy. ²Center for Human Genetic Research, Massachusetts General Hospital Research Institute and Department of Neurology, Harvard Medical School, 185 Cambridge Street, Boston, MA 02114, USA. ³Department of Molecular, Cell and Cancer Biology, University of Massachusetts Medical School, Worcester, MA 01605, USA.

Received: 15 March 2024 Accepted: 10 April 2025

Published online: 04 May 2025

References

- Biscotti MA, Olmo E, Heslop-Harrison JSP. Repetitive DNA in eukaryotic genomes. *Chromosome Res.* 2015;23:415–20.
- Liao X, Zhu W, Zhou J, Li H, Xu X, Zhang B, et al. Repetitive DNA sequence detection and its role in the human genome. *Commun Biol.* 2023;6:954.
- Cremer T, Cremer C. Chromosome territories, nuclear architecture and gene regulation in mammalian cells. *Nat Rev Genet.* 2001;2:292–301.
- Schneider R, Grosschedl R. Dynamics and interplay of nuclear architecture, genome organization, and gene expression. *Genes Dev.* 2007;21:3027–43.
- Wijmenga C, Hewitt JE, Sandkuijl LA, Clark LN, Wright TJ, Dauwerse HG, et al. Chromosome 4q DNA rearrangements associated with facioscapulohumeral muscular dystrophy. *Nat Genet.* 1992;2:26–30.
- Gabellini D, Green MR, Tupler R. Inappropriate gene activation in FSHD: a repressor complex binds a chromosomal repeat deleted in dystrophic muscle. *Cell.* 2002;110:339–48.
- Lemmers RJLF, Van Der Vliet PJ, Klooster R, Sacconi S, Camaño P, Dauwerse JG, et al. A unifying genetic model for facioscapulohumeral muscular dystrophy. *Science.* 2010;329:1650–3.
- Huichalaf C, Micheloni S, Ferri G, Caccia R, Gabellini D. DNA methylation analysis of the macrosatellite repeat associated with FSHD muscular dystrophy at single nucleotide level. *PLoS ONE.* 2014;9:e115278.
- Salsi V, Magdinier F, Tupler R. Does DNA methylation matter in FSHD? *Genes.* 2020;11:258.
- Nikolic A, Jones TI, Govi M, Mele F, Maranda L, Sera F, et al. Interpretation of the epigenetic signature of facioscapulohumeral muscular dystrophy in light of genotype-phenotype studies. *Int J Mol Sci.* 2020;21:2635.
- Van Overveld PGM, Enthoven L, Ricci E, Rossi M, Felicetti L, Jeanpierre M, et al. Variable hypomethylation of D4Z4 in facioscapulohumeral muscular dystrophy. *Ann Neurol.* 2005;58:569–76.
- Grow EJ, Weaver BD, Smith CM, Guo J, Stein P, Shadle SC, et al. p53 convergently activates Dux/DUX4 in embryonic stem cells and in facioscapulohumeral muscular dystrophy cell models. *Nat Genet.* 2021;53:1207–20.
- Erdmann H, Scharf F, Gehling S, Benet-Pagès A, Jakubiczka S, Becker K, et al. Methylation of the 4q35 D4Z4 repeat defines disease status in facioscapulohumeral muscular dystrophy. *Brain J Neurol.* 2022;146:1388.
- Gould T, Jones TI, Jones PL. Precise epigenetic analysis using targeted bisulfite genomic sequencing distinguishes FSHD1, FSHD2, and healthy subjects. *Diagnostics.* 2021;11:1469.
- Das S, Chadwick BP. Influence of repressive histone and DNA methylation upon D4Z4 transcription in non-myogenic cells. Kyba M, editor. *PLoS ONE.* 2016;11:e0160022.
- Vakoc CR, Mandat SA, Olenchok BA, Blobel GA. Histone H3 lysine 9 methylation and HP1 γ are associated with transcription elongation through mammalian chromatin. *Mol Cell.* 2005;19:381–91.
- Zeng W, De Greef JC, Chen YY, Chien R, Kong X, Gregson HC, et al. Specific loss of histone H3 lysine 9 trimethylation and HP1 γ /cohesin binding at D4Z4 repeats is associated with facioscapulohumeral dystrophy (FSHD). Ferguson-Smith AC, editor. *PLoS Genet.* 2009;5:e1000559.
- Cabianca DS, Casa V, Bodega B, Xynos A, Ginelli E, Tanaka Y, et al. A long ncRNA links copy number variation to a polycomb/trithorax epigenetic switch in FSHD muscular dystrophy. *Cell.* 2012;149:819–31.
- Campbell AE, Shadle SC, Jagannathan S, Lim J-W, Resnick R, Tawil R, et al. NuRD and CAF-1-mediated silencing of the D4Z4 array is modulated by DUX4-induced MBD3L proteins. *Elife.* 2018. <https://doi.org/10.7554/eLife.31023>.
- Salsi V, Vattemi GNA, Tupler RG. The FSHD jigsaw: are we placing the tiles in the right position? *Curr Opin Neurol.* 2023. <https://doi.org/10.1097/WCO.0000000000001176>.
- Snider L, Geng LN, Lemmers RJLF, Kyba M, Ware CB, Nelson AM, et al. Facioscapulohumeral dystrophy: incomplete suppression of a retrotransposed gene. *Pearson CE, editor. PLoS Genet.* 2010;6:1–14.
- Banerji CRS, Zammit PS. Pathomechanisms and biomarkers in facioscapulohumeral muscular dystrophy: roles of DUX4 and PAX7. *EMBO Mol Med.* 2021. <https://doi.org/10.15252/emmm.202013695>.
- Ricci G, Zatz M, Tupler R. Facioscapulohumeral muscular dystrophy: more complex than it appears. *Curr Mol Med.* 2014;14:1052–68.
- Ricci G, Scionti I, Sera F, Govi M, D'Amico R, Frambolli I, et al. Large scale genotype-phenotype analyses indicate that novel prognostic tools are required for families with facioscapulohumeral muscular dystrophy. *Brain.* 2013;136:3408–17.
- Salort-Campana E, Nguyen K, Bernard R, Jouve E, Solé G, Nadaj-Pakleza A, et al. Low penetrance in facioscapulohumeral muscular dystrophy type 1 with large pathological D4Z4 alleles: a cross-sectional multicenter study. *Orphanet J Rare Dis.* 2015;10:2.
- Goto K, Nishino I, Hayashi YK. Very low penetrance in 85 Japanese families with facioscapulohumeral muscular dystrophy 1A. *J Med Genet.* 2004;41:12e–12.
- Wohlgemuth M, Lemmers RJ, Jonker M, van der Kooi E, Horlings CG, van Engelen BG, et al. A family-based study into penetrance in facioscapulohumeral muscular dystrophy type 1. *Neurology.* 2018;91:e444–54.
- Wang Z, Qiu L, Lin M, Chen L, Zheng F, Lin L, et al. Prevalence and disease progression of genetically-confirmed facioscapulohumeral muscular dystrophy type 1 (FSHD1) in China between 2001 and 2020: a nationwide population-based study. *Lancet Reg Health West Pac.* 2022;18:100323.
- Scionti I, Greco F, Ricci G, Govi M, Arashiro P, Vercelli L, et al. Large-scale population analysis challenges the current criteria for the molecular diagnosis of facioscapulohumeral muscular dystrophy. *Am J Hum Genet.* 2012;90:628–35.
- Salsi V, Chiara M, Pini S, Kus P, Ruggiero L, Bonanno S, et al. A human pan-genomic analysis reconfigures the genetic and epigenetic make up of facioscapulohumeral muscular dystrophy [Internet]. *medRxiv.* 2023;41:10.
- Pastorello E, Cao M, Trevisan CP. Atypical onset in a series of 122 cases with FacioScapuloHumeral muscular dystrophy. *Clin Neurol Neurosurg.* 2012;114:230–4.
- Ruggiero L, Mele F, Manganello F, Bruzzese D, Ricci G, Vercelli L, et al. Phenotypic variability among patients with D4Z4 reduced allele facioscapulohumeral muscular dystrophy. *JAMA Netw Open.* 2020;3:e204040.
- Vercelli L, Mele F, Ruggiero L, Sera F, Tripodi S, Ricci G, et al. A 5-year clinical follow-up study from the Italian National Registry for FSHD. *J Neurol.* 2021;268:356–66.
- Sakellariou P, Kekou K, Fryssira H, Sofocleous C, Manta P, Panousopoulou A, et al. Mutation spectrum and phenotypic manifestation in FSHD Greek patients. *Neuromuscul Disord.* 2012;22:339–49.
- Zatz M, Marie SK, Passos-Bueno MR, Vainzof M, Campiotto S, Cerqueira A, et al. High proportion of new mutations and possible anticipation in Brazilian facioscapulohumeral muscular dystrophy families. *Am J Hum Genet.* 1995;56:99–105.
- Nakagawa M, Matsuzaki T, Higuchi I, Fukunaga H, Inui T, Nagamitsu S, et al. Facioscapulohumeral muscular dystrophy: clinical diversity and genetic abnormalities in Japanese Patients. *Intern Med.* 1997;36:333–9.
- Bettio C, Salsi V, Orsini M, Calanchi E, Magnotta L, Gagliardelli L, et al. The Italian National Registry for FSHD: an enhanced data integration and an analytics framework towards smart health care and precision medicine for a rare disease. *Orphanet J Rare Dis.* 2021;16:1.
- Zeng W, Chen YY, Newkirk DA, Wu B, Balog J, Kong X, et al. Genetic and epigenetic characteristics of FSHD-associated 4q and 10q D4Z4 that are distinct from Non-4q/10q D4Z4 homologs. *Hum Mutat.* 2014;35:998–1010.
- Mocciaro E, Giamb Bruno R, Micheloni S, Cernilogar FM, Andolfo A, Consonni C, et al. WDR5 is required for DUX4 expression and its pathological effects in FSHD muscular dystrophy. *Nucleic Acids Res.* 2023;51:5144–61.
- Lemmers RJLF, van der Vliet PJ, Blatnik A, Balog J, Zidar J, Henderson D, et al. Chromosome 10q-linked FSHD identifies DUX4 as principal disease gene. *J Med Genet.* 2022;59:180–8.

41. Robin JD, Ludlow AT, Batten K, Gaillard M-C, Stadler G, Magdiner F, et al. SORBS2 transcription is activated by telomere position effect-over long distance upon telomere shortening in muscle cells from patients with facioscapulohumeral dystrophy. *Genome Res.* 2015;25:1781–90.
42. Cortesi A, Pesant M, Sinha S, Marasca F, Sala E, Gregoretti F, et al. 4q–D4Z4 chromatin architecture regulates the transcription of muscle atrophic genes in facioscapulohumeral muscular dystrophy. *Genome Res.* 2019;29:883–95.
43. Robin JD, Ludlow AT, Batten K, Magdiner F, Stadler G, Wagner KR, et al. Telomere position effect: regulation of gene expression with progressive telomere shortening over long distances. *Genes Dev.* 2014;28:2464–76.
44. Jones TI, Chen JCJ, Rahimov F, Homma S, Arashiro P, Beermann ML, et al. Facioscapulohumeral muscular dystrophy family studies of DUX4 expression: Evidence for disease modifiers and a quantitative model of pathogenesis. *Hum Mol Genet.* 2012;21:4419–30.
45. Jones TI, King OD, Himeda CL, Homma S, Chen JCJ, Beermann ML, et al. Individual epigenetic status of the pathogenic D4Z4 macrosatellite correlates with disease in facioscapulohumeral muscular dystrophy. *Clin Epigenet.* 2015;7:37.
46. Crispatsu G, Rehimi R, Pachano T, Bleckwehl T, Cruz-Molina S, Xiao C, et al. The chromatin, topological and regulatory properties of pluripotency-associated poised enhancers are conserved in vivo. *Nat Commun.* 2021;12:4344.
47. Boltsis I, Grosveld F, Giraud G, Kolovos P. Chromatin conformation in development and disease. *Front Cell Dev Biol.* 2021. <https://doi.org/10.3389/fcell.2021.723859>.
48. Becker JS, McCarthy RL, Sidoli S, Donahue G, Kaeding KE, He Z, et al. Genomic and proteomic resolution of heterochromatin and its restriction of alternate fate genes. *Mol Cell.* 2017;68:1023–1037.e15.
49. Ernst J, Kheradpour P, Mikkelsen TS, Shoresh N, Ward LD, Epstein CB, et al. Mapping and analysis of chromatin state dynamics in nine human cell types. *Nature.* 2011;473:43–9.
50. Kondo T, Bobek MP, Kuick R, Lamb B, Zhu X, Narayan A, et al. Whole-genome methylation scan in ICF syndrome: Hypomethylation of non-satellite DNA repeats D4Z4 and NBL2. *Hum Mol Genet.* 2000;9:597–604.
51. Yang F, Zhang L, Li J, Huang J, Wen R, Ma L, et al. Trichostatin A and 5-azacytidine both cause an increase in global histone H4 acetylation and a decrease in global DNA and H3K9 methylation during mitosis in maize. *BMC Plant Biol.* 2010;10:178.
52. Rymarchyk S, Kang W, Cen Y. Substrate-dependent sensitivity of SIRT1 to nicotinamide inhibition. *Biomolecules.* 2021;11:312.
53. Rouleau M, Patel A, Hendzel MJ, Kaufmann SH, Poirier GG. PARP inhibition: PARP1 and beyond. *Nat Rev Cancer.* 2010;10:293–301.
54. Zha S, Wang F, Li Z, Ma Z, Yang L, Liu F. Pj34, a PARP1 inhibitor, promotes endothelial repair in a rabbit model of high fat diet-induced atherosclerosis. *Cell Cycle.* 2019;18:2099–109.
55. Ying W, Alano CC, Garnier P, Swanson RA. NAD⁺ as a metabolic link between DNA damage and cell death. *J Neurosci Res.* 2005;79:216–23.
56. Basu A, Krishnamurthy S. Cellular responses to cisplatin-induced DNA damage. *J Nucleic Acids.* 2010;2010:201367.
57. Wei F, Hao P, Zhang X, Hu H, Jiang D, Yin A, et al. Etoposide-induced DNA damage affects multiple cellular pathways in addition to DNA damage response. *Oncotarget.* 2018;9:24122–39.
58. Masteika IF, Sathya A, Homma S, Miller BM, Boyce FM, Miller JB. Downstream events initiated by expression of FSHD-associated DUX4: Studies of nucleocytoplasmic transport, γ H2AX accumulation, and Bax/Bak-dependence. *Biol Open.* 2022. <https://doi.org/10.1242/bio.059145>.
59. Broucqsaault N, Morere J, Gaillard M-C, Dumonceaux J, Torrents J, Salort-Campana E, et al. Dysregulation of 4q35- and muscle-specific genes in fetuses with a short D4Z4 array linked to facio-scapulo-humeral dystrophy. *Hum Mol Genet.* 2013;22:4206–14.
60. Gaillard MC, Broucqsaault N, Morere J, Laberthonnière C, Dion C, Badja C, et al. Analysis of the 4q35 chromatin organization reveals distinct long-range interactions in patients affected with Facio-Scapulo-Humeral Dystrophy. *Sci Rep.* 2019. <https://doi.org/10.1038/s41598-019-46861-x>.
61. Timinszky G, Till S, Hassa PO, Hothorn M, Kustatscher G, Nijmeijer B, et al. A macrodomain-containing histone rearranges chromatin upon sensing PARP1 activation. *Nat Struct Mol Biol.* 2009;16:923–9.
62. Kozlowski M, Corujo D, Hothorn M, Guberovic I, Mandemaker IK, Blessing C, et al. MacroH2A histone variants limit chromatin plasticity through two distinct mechanisms. *EMBO Rep.* 2018. <https://doi.org/10.15252/embr.201744445>.
63. Klooster R, Straasheijm K, Shah B, Sowden J, Frants R, Thornton C, et al. Comprehensive expression analysis of FSHD candidate genes at the mRNA and protein level. *Eur J Hum Genet.* 2009;17:1615–24.
64. Rijkers T, Deidda G, Van Koningsbruggen S, Van Geel M, Lemmers RULF, Van Deutekom JCT, et al. FRG2, an FSHD candidate gene, is transcriptionally upregulated in differentiating primary myoblast cultures of FSHD patients. *J Med Genet.* 2004;41:826–36.
65. Bodega B, Ramirez GDC, Grasser F, Cheli S, Brunelli S, Mora M, et al. Remodeling of the chromatin structure of the facioscapulohumeral muscular dystrophy (FSHD) locus and upregulation of FSHD-related gene 1 (FRG1) expression during human myogenic differentiation. *BMC Biol.* 2009;7:41.
66. Bouju S, Piétu G, Le Cunff M, Cros N, Malzac P, Pellissier JF, et al. Exclusion of muscle specific actinin-associated LIM protein (ALP) gene from 4q35 facioscapulohumeral muscular dystrophy (FSHD) candidate genes. *Neuromuscul Disord.* 1999;9:3–10.
67. Xia H, Winokur ST, Kuo WL, Altherr MR, Bredt DS. Actinin-associated LIM protein: identification of a domain interaction between PDZ and spectrin-like repeat motifs. *J Cell Biol.* 1997;139:507–15.
68. Masny PS, Chan OYA, de Greef JC, Bengtsson U, Ehrlich M, Tawil R, et al. Analysis of allele-specific RNA transcription in FSHD by RNA-DNA FISH in single myonuclei. *Eur J Hum Genet.* 2010;18(448–56):69.
69. Sutcu HH, Rassinoux P, Donnio L-M, Neuillet D, Vianna F, Gabillot O, et al. Decline of DNA damage response along with myogenic differentiation. *bioRxiv.* 2023;187:127. <https://doi.org/10.1101/2023.06.27.546688v1>.
70. Bensaude O. Inhibiting eukaryotic transcription. *Transcription.* 2011;2:103–8.
71. Frank L, Rippe K. Repetitive RNAs as regulators of chromatin-associated subcompartment formation by phase separation. *J Mol Biol.* 2020;432:4270–86.
72. Chu HP, Cifuentes-Rojas C, Kesner B, Aeby E, Goo LH, Wei C, et al. TERRA RNA antagonizes ATRX and protects telomeres. *Cell.* 2017;170:86–101.e16.
73. Mondal T, Subhash S, Kanduri C. Chromatin RNA immunoprecipitation (ChRIP). *Methods Mol Biol.* 2018;1689:65–76.
74. West JA, Davis CP, Sunwoo H, Simon MD, Sadreyev RI, Wang PI, et al. The long noncoding RNAs NEAT1 and MALAT1 bind active chromatin sites. *Mol Cell.* 2014;55:791–802.
75. Nurk S, Koren S, Rhie A, Rautiainen M, Bizkadez AV, Mikheenko A, et al. The complete sequence of a human genome. *Science.* 2022;376:44–53.
76. de Koning APJ, Gu W, Castoe TA, Batzer MA, Pollock DD. Repetitive elements may comprise over two-thirds of the human genome. *Copenhaver GP, editor. PLoS Genet.* 2011;7:e1002384.
77. Smit AF. Interspersed repeats and other mementos of transposable elements in mammalian genomes. *Curr Opin Genet Dev.* 1999;9:657–63.
78. Dumbovic G, Forcales SV, Perucho M. Emerging roles of macrosatellite repeats in genome organization and disease development. *Epigenetics.* 2017;12:515–26.
79. Brahmachary M, Guilmatre A, Quilez J, Hasson D, Borel C, Warburton P, et al. Digital genotyping of macrosatellites and multicopy genes reveals novel biological functions associated with copy number variation of large tandem repeats. *Orr HT, editor. PLoS Genet.* 2014;10:e1004418.
80. Stankiewicz P, Lupski JR. Structural variation in the human genome and its role in disease. *Annu Rev Med.* 2010;61:437–55.
81. Salsi V, Ferrari S, Ferraresi R, Cossarizza A, Grande A, Zappavigna V. HOXD13 binds DNA replication origins to promote origin licensing and is inhibited by geminin. *Mol Cell Biol.* 2009;29:5775–88.

Publisher's Note

Springer Nature remains neutral with regard to jurisdictional claims in published maps and institutional affiliations.